Polymer Composites

WILEY | spe INSPIRING PLASTICS PROFESSIONALS

RESEARCH ARTICLE

The Combined Effects of Hybrid HNTs and Pure Boron Nanoparticles on Shear Strength and Failure Characteristics of Adhesive Joints

Gülağa Taş[1] | Mehmet Veysel Çakır[2]

[1]Aeronautics and Aerospace Engineering Department, Hasan Kalyoncu University, Gaziantep, Turkey | [2]Department of Mechanical Engineering, Kilis 7 Aralık University, Kilis, Turkey

Correspondence: Gülağa Taş (agatas@hku.edu.tr)

Received: 10 October 2025 | **Revised:** 20 November 2025 | **Accepted:** 30 November 2025

Keywords: boron nanoparticles | fracture mechanisms | halloysite nanotube | shear strength | synergistic effect

ABSTRACT

This study investigates the effect of a hybrid incorporation of halloysite nanotubes (HNT) and pure boron nanoparticles (BNP) on the shear strength of single-lap joints bonded with Araldite 2014 epoxy adhesive. The adhesive matrix used in this study is an epoxy-based Araldite 2014. Hybrid-doped joints containing 1.2% HNT and 0.3% BNP by weight demonstrated a 48.94% increase in maximum shear strength compared to the pure specimen. The most significant displacement at rupture—approximately 2.5 mm—was observed in these specimens, resulting in a 72.41% increase in ductility relative to the pure adhesive. Fracture mode analysis revealed a transition from adhesive failure in pure samples to cohesive failure and fiber tearing in nanoparticle-doped samples, indicating enhanced adhesion between the adhesive and substrates. Detailed Scanned Electron Microscopy (SEM) analyses showed that HNT particles increase toughness through crack-bridging, while BNP particles enhance toughness via crack-deviation and particle segregation mechanisms; together, these effects provide a synergistic toughening mechanism. Additionally, Fourier Transform Infrared (FTIR) analyses demonstrated that chemical interactions between nanoparticles and the Araldite 2014 matrix further improve adhesive strength. These findings contribute to the development of high-performance epoxy adhesive formulations for structurally demanding applications.

1 | Introduction

Due to advantages such as no residual stress generation, uniform stress distribution, no stress concentration zones, light weight, environmental friendliness, and so forth, adhesively bonded joints (ABJ)—connections formed by gluing two or more surfaces together—are superior to classical joining processes (welding and mechanical joining). Thus, adhesively bonded joints are gaining importance in many automotive, marine, and aviation industries. ABJs can be applied to bind materials regardless of thickness, shape, or type [1–8].

Comprehensive structural improvement studies have played a key role in advancing adhesive joint strength. These go beyond just nanostructure or adhesive interactions. Researchers have examined the comparative strength effects of laminate composite patches on double-strap joints under tensile loading [9]. Further research has focused on how different joint geometries—such as one step-lap joint, double-strap joint, and stepped double-strap joint—affect joint strength under the same adhesive area [10]. Investigations also highlight the significant role of combining thin-walled inserts with nanostructure-reinforced adhesives. This approach

Highlights

- Hybrid HNT/BNP fillers significantly enhanced the shear strength of epoxy joints.
- Optimum ratio provided ~50% strength and ~70% ductility improvement.
- Failure mode shifted from adhesive to cohesive and fiber-tear.
- SEM showed toughening via crack-bridging (HNT) and crack-deviation (BNP).
- FTIR confirmed chemical interactions between nanoparticles and the epoxy.

structurally tunes the flexural performance of single-lap joints [11].

Moreover, ABJs can be used without damaging the adherends, unlike mechanical joining processes [12–15]. The main drawback of ABJs is their lower adhesion strength compared to that of the adherends. The literature shows that researchers have proposed adding micro- or nanoparticles—either as fibers or particles—to the adhesive to enhance the strength of ABJs while maintaining the physical and chemical properties of both the adhesive and the new phase [16–18]. Experimental studies have demonstrated that incorporating carbon nanostructures (graphene, carbon nanotube-COOH, and fullerene C60) into structural adhesives increases not only the strength under static load but also the static strength after fully reversed fatigue loading [19]. Additionally, recent efforts have focused on activating nanostructures or fibers via chemical surface modifications (such as oxidation and silanization) to improve the adhesive's internal bond (cohesion) strength [20]. These studies revealed that carbon fiber reinforcements (1–4 wt%) with chemical surface treatments can significantly increase the nominal maximum tensile value of the adhesive (up to 177%) and that bond performance can be further enhanced depending on the type of chemical modification [21]. Notably, hybrid approaches that combine surface treatments (chemical etching or anodization) of the adherend with nanostructure reinforcements in the adhesive have provided synergistic benefits, maximizing bond strength [22].

Nanoparticles, which primarily serve as bridges between the molecules and atoms of the parent material to which they are attached, are microscopic particles with sizes less than 100 nm and can possess various compositions and morphologies [23]. Furthermore, nanoparticles have fewer defects, lower specific surface energy, and a smaller surface area than their macro forms [17]. One method for improving the mechanical properties of adhesively bonded joints is to add nanoparticles with different geometries, such as planar, spherical, or tubular [24].

In subsequent studies, basic parameters affecting the strength of adhesive connections, such as the type, size, and nanoparticle additive ratio, were investigated. For example, Zhai et al. studied the effects of nano-Al_2O_3 (average diameter of 80 nm), nano-$CaCO_3$ (40–80 nm), and nano-SiO_2 (10–20 nm), together with the surface roughness of the adherents (silicon carbide paper, 60 grit (60#) and 150 grit (150#)). They obtained greater improvements in the adhesive joint of Al_2O_3 with the silicon carbide paper of 150 grit, which is 5 times higher than that of pristine epoxy [25]. Borghei et al. [26], studied the lap-shear strength of ABJs by mixing two graphene nanoparticle (GNP) types with Araldite 2011 adhesive. They concluded that the increment of shear strength of adhesive joints is 24% for type II (smaller size) and 12% for type I relative to the joints bonded with pristine adhesive. Also, they noted that a higher increment for type II was due to a more homogeneous distribution of it in the adhesive. Saraç et al. [27], in the study they performed, added nano-Al_2O_3, nano-TiO_2, and nano-SiO_2 into the adhesive separately. They found that the maximum loadings for the nanoparticle additives are 4%, 6%, and 4% by weight for nano-Al_2O_3, nano-SiO_2, and nano-TiO_2, respectively. The effect of multiwalled carbon nanotubes (MWCNT), nano silica (NS), and nano clay (NC) on the bonding strength of single-lap joint adhesively bonded joints has been investigated in a study by Cakir and Kinay [28]. In the study, epoxy was used as an adhesive, and glass fiber-reinforced polymer (GFRP) was used as plates. They stated that bonding strength increased by roughly 62% for 0.5 wt.% MWCNTs, 37.8% for 1.5 wt.% NC, and 43.3% for 1.5 wt.% NS. In the study conducted by Akpınar et al. [29], fullerene nanoparticles, graphene nanoparticles, and carbon nanotubes were used as adhesive fillers. The researchers reported that the maximum load was obtained by adding 1% by weight for each adhesive filler. Bali and Topkaya [30] investigated the tensile fatigue behavior of adhesively bonded single-lap joints. The study used graphene nanoparticles (GNP) as an adhesive filler at different weight fractions. It was stated that the highest fatigue life was obtained with 0.5 wt% GNP fillers in the adhesive. Soltannia and Taheri [31] investigated and compared the effects of graphitized carbon fibers, multiwalled carbon nanotubes, and nanographene particles on mechanical properties, including tensile and impact, in single-lap adhesive bonding of glass/epoxy and graphite/epoxy plates. While all nanoparticle-doped samples showed better mechanical properties than pure samples, the greatest improvements were observed in nanographene samples. Nano boron particles are promising fillers for adhesively bonded joints. The durability and resistance to environmental factors, such as temperature changes, moisture, and radiation, of adhesively bonded joints can be enhanced by adding n-BN particles. Also, the high surface area of boron nitride particles provides stress transfer from the adhesive to the adherents. As a result, the mechanical properties of the bond increase significantly [32–35].

Research on the effect of nanoparticles on the strength of adhesively bonded joints has mainly concentrated on single-phase nanoparticles. However, only a limited number of studies investigate the impact of hybrid nanoparticle combinations on adhesive joints containing multiple nanoparticle types. Some notable examples include:

Özbek and Çakır examined the shear and flexural strength of adhesively bonded single-lap joints by hybridizing MWCNTs with silica nanoparticles at various concentrations [36]. They discovered that the highest shear and flexural strength was achieved by mixing 0.5 wt% MWCNT with 0.25 wt% silica nanoparticles in the adhesive. Zamani et al. [24] compared fatigue failure under four-point bending in ABJs using single-phase GNP,

single-phase nano-silica, and a hybrid nanoparticle combination of GNP and silica (GNP + SIO_2). Their findings indicated that the fatigue life of ABJs with 1.5 wt.% hybrid nanoparticles was 44.92% and 67.28% longer than those with single GNP and single nano-silica, respectively. Razavi et al. [37]. explored the synergistic effect of MWCNT and nano-silica in a 1:1 weight ratio, comparing this combination to their individual effects. They concluded that the synergistic effect was more significant than the separate effects when the weight ratio was equal. The study reported the most tremendous improvements in shear strength and elongation at 28% and 36%, respectively, at a nanoparticle concentration of 0.8% by weight. In research conducted by Rao et al. [38], the collaborative effect of MWCNT and GNP on single-lap joints (SLJs) was investigated. The results showed the most significant improvements in shear strength (36.6%) and elongation (33.2%) at a MWCNT-to-GNP weight ratio of 0.75 wt%. Zamani et al. [39] further examined the synergistic effect of GNP and nanosilica, finding that mixing 0.5 wt.% of both nanoparticles resulted in a higher static failure load and a longer fatigue life. Lastly, Çakır [13] studied the synergistic effect of nano-silica and GNP additives on the flexural strength and toughening mechanisms of ABJs, concluding that the best performance was observed in samples with 1.5 wt% nano-silica and 0.5 wt% GNP.

Research on pure BNPs remains limited compared to the more extensively studied boron-containing compounds, such as boron nitride (BN) and boron carbide (B_4C) [40]. While BN particles are considered promising fillers due to their high surface area, potential to increase durability, and ability to improve stress transfer mechanisms [26–29], there are not enough published studies, except for one using pure BNPs as structural reinforcement in adhesives [41]. Previous research has predominantly focused on single-phase nanoparticles to improve adhesive properties, resulting in a critical gap in understanding the impact of hybrid nanostructure combinations, particularly those involving underexplored materials such as BNPs. Additionally, studies indicate that incorporating HNTs into adhesive matrices can significantly improve the mechanical properties of adhesive joints, including increased tensile, fracture, and shear strengths [42, 43]. However, the combined use of HNTs and BNPs in adhesives has not been directly investigated in the literature. Addressing this gap, the present study systematically examines the synergistic effect of combining HNTs and pure BNPs in adhesively bonded joints. By leveraging their complementary toughening mechanisms, the study seeks to determine the optimal hybrid ratio for enhanced mechanical performance. These findings are anticipated to contribute to the development of high-performance adhesive formulations for structurally demanding applications.

2 | Materials and Methods

2.1 | Materials

This study used the adhesive Araldite 2014-2, a product of Huntsman Advanced Materials Americas LLC, Canada. It is environmentally friendly, room-temperature curing, two-component, chemical-resistant, and high-viscosity epoxy-based. The GFRP composite plates were obtained from Küçükparmak Mühendislik San Tic. Ltd., Turkey, and were 2 mm thick. The mechanical properties of Araldite 2014-2 and GFRP composite are given in Table 1.

HNT particles, first identified as a clay mineral by Berthier in 1826, are abundantly found in mineral deposits worldwide and are aluminosilicate clay minerals [44, 45]. HNT particles are in the form of tubes and are also considered a promising alternative material, with economical, easy availability compared to carbon nanotube particles [45, 46]. The physical properties of halloysite nanotubes used in this study are given in Table 2.

The pure BNPs were purchased from Nanografi Nano Technology Co. in Turkey. Table 3 presents the physical properties of BNPs.

2.2 | Sample Preparation

GFRP plates, measuring 100 mm in length and 25 mm in width, were prepared by cutting them with a guillotine. To enhance adhesion between the adhesive and the GFRP plates, the bonding area was roughened with 100-grit silicon carbide sandpaper in accordance with ISO 17212. After abrading, the surfaces were thoroughly cleaned with acetone to remove any chemical and physical impurities. Finally, the GFRP plates were soaked in distilled water and dried in an oven for 30 min at 40°C.

To investigate the synergistic effect of HNTs and BNPs, the maximum weight ratio of each particle that significantly affects the

TABLE 1 | Mechanical properties of Araldite 2014–2 and GFRP composite.

Materials	Density (g/cm^3)	Tensile strength (Mpa)	Modulus of elasticity (GPa)
GFRP composite	1.82	362	18.65
Araldite 2014-2	2.77	30	3.1

TABLE 3 | Physical properties of pure boron nanoparticles.

	Purity	Density (g/cm^3)	Average size (nm)	Crystal structure
Nano-boron	99.85%	3.58	100	Hexagonal

TABLE 2 | Physical properties of HNT.

	Density (g/cm^3)	Surface area (m^2/g)	Average length (μm)	Average outside diameter (nm)	Average inner diameter (nm)
HNT	2.6	> 65	1.2	40	20

shear strength of SLJs was determined. The maximum weight ratio for HNT was set at 2%, consistent with findings by Özbek et al. [43]. In our preliminary studies with BNPs, the optimal weight ratio was 0.4% [41]. Given the lower weight ratio of boron nanoparticles and their higher cost compared to HNT, the mixture's composition was adjusted by varying the HNT weight ratio. In contrast, the boron content was set at 0.3%. The composition of the mix, including the adhesive and nanoparticles, is detailed in Table 4.

Ingredients were weighed on a precision balance to prepare the adhesive mixture. To ensure homogeneous distribution of nanoparticles and minimize standard deviation in the final joints, the operative addition technique described by Gültekin et al. [47] was used. Equal amounts of Araldite 2014-2 and acetone were combined in a glass beaker to reduce adhesive viscosity. Nanoparticles were then added, and the mixture was stirred with a Bandelin Sonopuls series 4000 ultrasonic homogenizer at 20 kHz and 60 W for about 60 min. The glass beaker was kept in an ice box to prevent premature curing, as shown in Figure 1. This process was repeated for each sample set.

TABLE 4 | The composition of the nanoparticle and adhesive mix.

Samples name	Percentage weight of the components		
	Halloysite nanotube	Nano boron	Araldite 2014-2
S	—	—	100
2H	2	—	98
4B	—	0.4	99.6
6H3B	0.6	0.3	99.1
9H3B	0.9	0.3	98.8
12H3B	1.2	0.3	98.5
15H3B	1.5	0.3	98.2

After mixing, the adhesive mixture was placed in a vacuum degasser for about 10 min at −0.75 bar and 22°C to allow acetone to evaporate. After degassing, the adhesive mixture was weighed to verify that no acetone remained. The complete evaporation of the acetone was controlled by measuring the amount of epoxy and nanostructure using a precision balance. While this process provided gravimetric control, the full chemical validation of acetone removal was achieved through subsequent FTIR spectroscopy.

During the final sample preparation stage, GFRP plates were positioned in a custom-designed aluminum mold (Figure 2a) that maintained a bonding area of $25 \times 25\,mm^2$ and an adhesive thickness of 0.2 mm. The mold was fabricated to ensure the total thickness of the overlapped joint remained consistently at 4.2 mm. A controlled weight was applied to the top of the mold to maintain uniform adhesive thickness. After 24 h in the mold, the samples underwent post-curing at 40°C for 16 h. Upon completion of curing, the overlap length and adhesive thickness of each specimen were measured and recorded with a precision digital micrometer before testing to confirm dimensional consistency. For each configuration, five

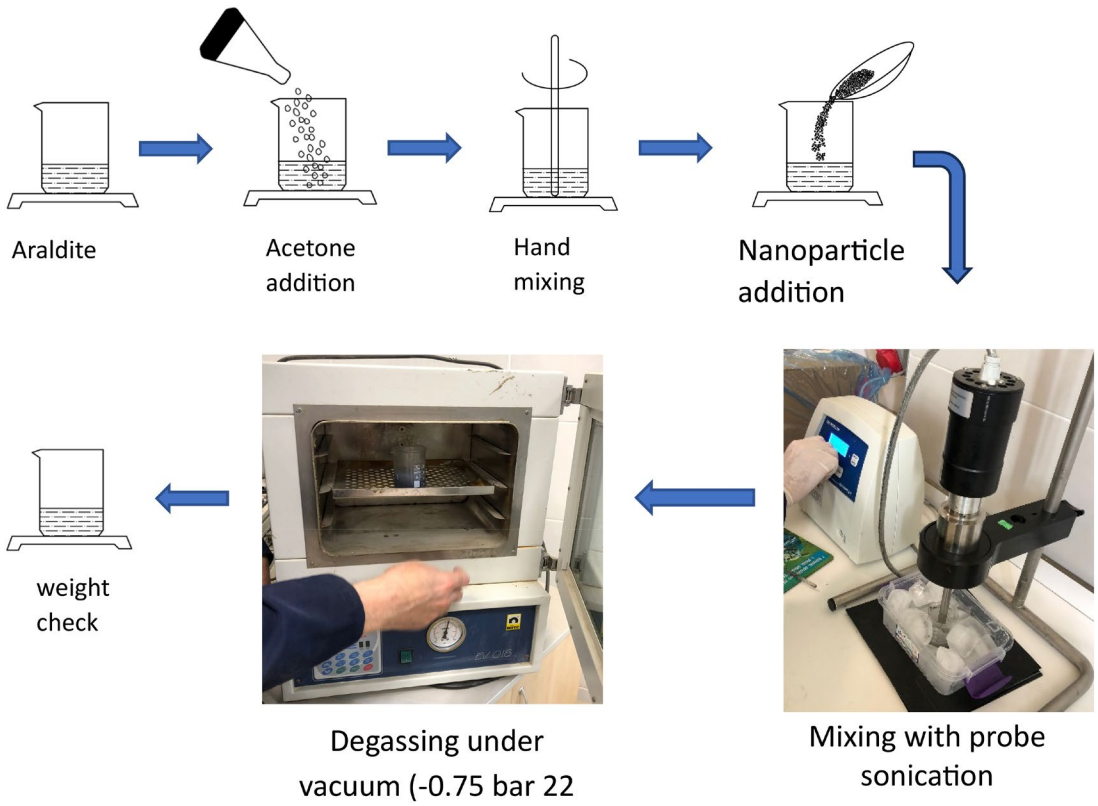

FIGURE 1 | The mixing process of adhesive doped with nanoparticles.

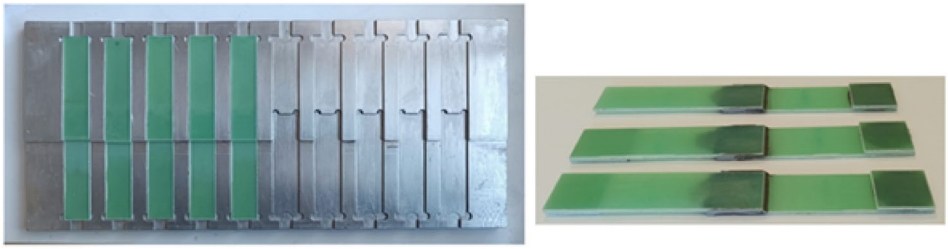

FIGURE 2 | (a) Aluminum mold, (b) fabricated samples.

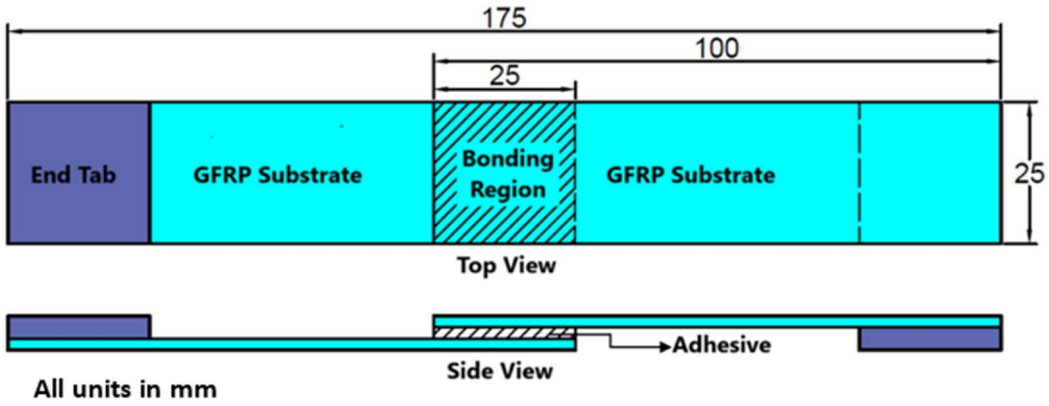

FIGURE 3 | View of the adhesively bonded single-lap joints.

TABLE 5 | Maximum load, shear strength, and % improvement values obtained from lap shear tests.

Samples	Average load (N)	Maximum shear strength (MPa)	% improvement
Pure	5397.25 ± 150.7	8.64 ± 0.24	0
2H	7086.61 ± 218.9	11.34 ± 0.35	**31.30**
4B	6949.66 ± 142.0	11.12 ± 0.23	**28.76**
6H3B	6808.00 ± 177.9	10.59 ± 0.28	22.64
9H3B	6864.88 ± 180.5	10.94 ± 0.29	26.67
12H3B	8038.66 ± 146.6	12.86 ± 0.23	**48.94**
15H3B	6516.36 ± 270.8	10.43 ± 0.43	20.72

Note: Bold values indicate the percentage of improvement in shear strength of the joints with respect to pure araldite 2014-2.

single-lap joint samples are fabricated. Representative samples are shown in Figure 2b.

2.3 | Lap-Shear Test

End tabs made from GFRP were attached to the samples to eliminate additional effects and ensure that a pure shear load was achieved, as illustrated in Figure 3. The lap-shear tests were performed using a Shimadzu AG-X Series testing machine to assess the impact of nanoparticles on the mechanical performance of the samples, in accordance with ASTM D5868-01.

Five samples were subjected to the lap-shear test for each configuration to ensure consistency and accuracy. The following formula was used to calculate the joints' maximum shear strength.

$$\tau_{\max} = \frac{P}{A}$$

where P is the maximum load and A is the area of the bonding region.

2.4 | FTIR Spectroscopy of Pure Adhesive and Doped Adhesive

FTIR Spectra of pure and doped adhesives were obtained using a Shimadzu IRSpirit-X spectrometer to examine whether new

bonds form. The number of scans was set to 32 to achieve a good signal-to-noise ratio (SNR). For solid and liquid materials, it is recommended to choose a resolution value between 4 and 8 cm^{-1}; thus, the resolution was set to 6 cm^{-1} [48].

3 | Results and Discussion

3.1 | Single-Lap Shear Test Results

The lap-shear test results for GFRP-GFRP adhesive joints prepared with single-phase, pure, and hybrid nanoparticle additives to Araldite 2014 adhesive are presented in Table 5 and Figure 4. The average tensile load for the single-phase HNT-doped sample (2H) was 7086.61 N, while the average tensile load for the 0.4 wt.% BNP-doped sample (4B) was 6949.66 N. In contrast, the average tensile load of the pure sample was 5397.25 N. The shear strengths of the single-phase specimens were 11.34 MPa for HNT and 11.12 MPa for BNP, representing improvements of 31.3% and 28.76%, respectively, over the undoped specimens. The hybrid nanoparticle-doped specimens 6H3B, 9H3B, 12H3B, and 15H3B, with HNT-to-BNP ratios of 2:1, 3:1, 4:1, and 5:1, respectively, also exhibited increased joint strength compared to the pure specimens. Specifically, the strength improvements for the 6H3B and 9H3B specimens were 22.64% and 26.67%, respectively. The 12H3B hybrid-doped specimen demonstrated the maximum enhancement, achieving a shear strength of 12.86 MPa and an average tensile load of 8038.66 N. It refers to a 48.94% increase in shear strength over the pure specimen, which was 13.4% more than the single-phase HNT-doped specimen (2H). These results indicate that the hybrid doping of HNT and BNP at the appropriate ratio can significantly enhance the performance of adhesive joints through a synergistic effect. However, further

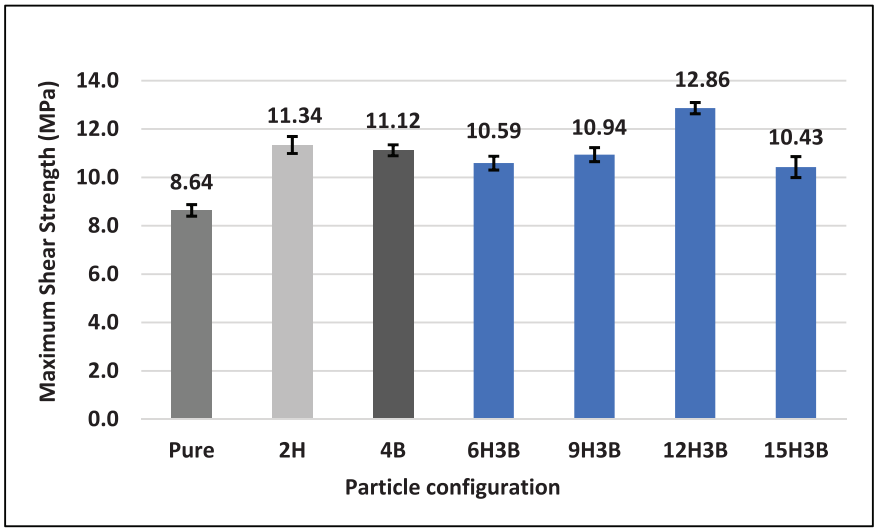

FIGURE 4 | Shear strength values obtained from lap-shear tests.

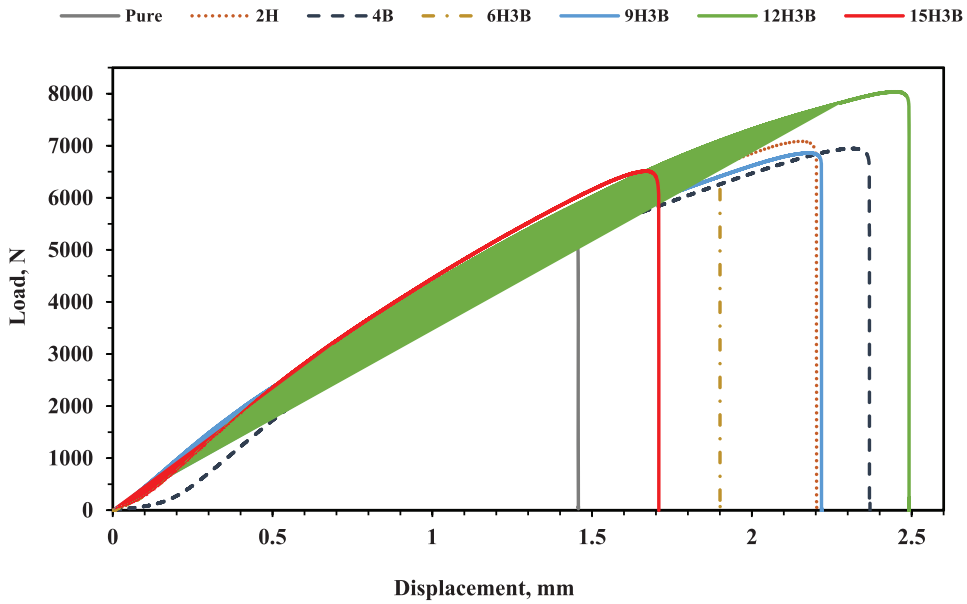

FIGURE 5 | Load–displacement graphics of samples.

increasing the HNT doping led to decreased shear strength, as observed in specimen 15H3B. This reduction can be attributed to particle agglomeration due to excessive doping, non-homogeneous dispersion, and microstructural defects that negatively impact load transfer.

Figure 5 presents the load–displacement curves obtained from lap-shear tests conducted on adhesive joints with different configurations. The displacement value at break load for the pure adhesive specimen is approximately 1.45 mm, less than that of all nanoparticle-doped specimens. Including nanoparticles enhances the adhesive matrix's ductility, whereas the pure adhesive exhibits a brittle structure. The break displacements for the 2H and 4B modified adhesives are nearly identical, around 2.21 mm. Compared to the pure specimens, the ductility of the modified adhesives improved by 52.41%. Since the peak load value for specimen 2H is higher, it is tougher than that of the 4B sample. Specifically, the 12H3B specimen demonstrates the highest peak load (around 8000 N) and displacement (approximately 2.5 mm). The combination of 1.2% HNT and 0.3% BNP additive led to significant improvements: a 48.94% increase in shear strength and a 72.41% increase in **ductility** compared to the pure sample. The toughness of adhesive connections can be qualitatively evaluated by the total energy absorbed before catastrophic damage, as indicated by the area under the experimental load–displacement curve [39, 49]. Therefore, this significant increase in ductility and the higher peak load indicate a substantial improvement in the strength or energy-absorption capacity of the joints, that is, their toughness. This suggests that the optimal ratio of hybrid HNT and BNP doping exhibits a synergistic effect, enhancing stress transfer and energy dissipation. However, weak interactions between the GFRP surfaces and polymer chains at low particle concentrations could limit overall deformation, thereby reducing the plastic strain capacity, as observed in the hybrid samples 6H3B and 9H3B [50, 51]. Additionally, excessive additive content, similar to that in the 15H3B specimen, may lead to embrittlement, resulting in reduced load and premature crack initiation [50, 52].

3.2 | Analysis of Failure Surfaces

3.2.1 | Macro Views

In this section, the unaided eye examined macro views of the damaged surfaces of adhesive joints with different nanoparticle additive configurations. According to ASTM D5573-99, the failure modes of adhesive joints made with fiber-reinforced polymer substrates are divided into seven classes [53]. The failure mode indicates the quality of adhesive joints and the bond strength. The distribution of load and stress between two bonded components enables the correct evaluation of failure modes [54]. Figure 6 shows that the adhesive layer remains on the surface of one of the adherents for joints made with pure adhesive. This damage type, called adhesive failure mode (AF), indicates poor interaction between the adhesive and the adherents, resulting in low bond performance. This type of failure is highly undesirable because the bond (chemical and mechanical) that should firmly bind the adhesive and the adherent is lost, leading to significant separation at the interface between the two materials [54]. This situation explains why the mechanical test results of the samples made with pure Araldite 2014 adhesive are lower than those of the others.

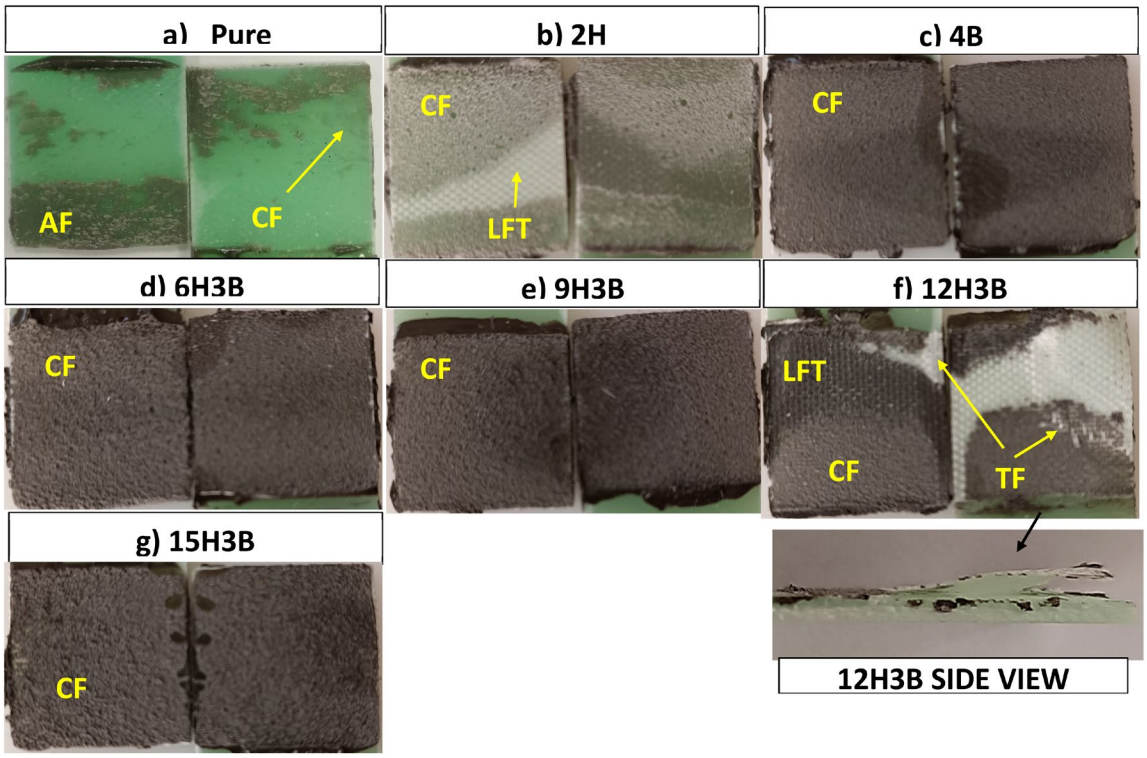

FIGURE 6 | Macro failure surfaces: (a) Pure: Adhesive failure (AF), (b) 2H: Cohesive failure (CF) + light fiber tear (LFT), (c) 4B: CF, (d) 6H3B: CF, (e) 9H3B: CF, (f) 12H3B: CF + fiber tear failure (TF), (g) 15H3B: CF.

Although the adhesive layer remained on substrates in a small amount on the failure surfaces of the samples made with pure Araldite 2014 adhesive, almost the entire surface of the 4B, 6H3B, 9H3B, and 15H3B samples indicates that the failure occurred within the adhesive itself. This failure, defined as cohesive failure (CF), occurs in a plane inside the adhesive layer and indicates that the adhesive adheres well to the substrates. This type of failure means that the adhesion to the substrate exceeds the adhesive's internal bond strength. It also shows strong interfacial reactions at the adhesive/substrate interface. In cohesive failure, the material's maximum strength is reached before rupture. Therefore, this is an ideal type of failure. Although it is better than adhesive failure, this type of failure is also undesirable in practical applications, as the adhesive remains the weakest part of the joint [54].

When the damaged appearance of the 2.0% HNT-doped sample is examined, it is evident that the dominant failure type is cohesive failure (CF). However, reinforcement fibers are observed in the GFRP matrix near the interface, and surface tearing is present in the substrate. The ASTM 5573 standard defines this type of failure as light fiber tearing (LFT). On the damaged surfaces of the 1.2% HNT and 0.3% nano boron doped samples, irregularly broken glass fibers were observed on both broken surfaces in the GFRP matrix. Fiber tear failure (TF) is thought to be caused by shear deformation occurring in the regions where load transfer occurs from the adhesive layer to the substrate [55]. Fiber tear failure (TF) means that the joint is not only damaged, but the damage involves the bonded material [56]. LFT and TF failures, which develop as the rupture of the bonded layer itself, indicate that high shear stresses are reached during loading. The interlayer delamination (Figure 6, side view) and yarn ruptures, together with fiber ruptures in the 2H and hybrid 12H3B samples with the best bonding performance, support the superior bonding performance of these joints (Table 5). When compared to the joints made with pure Araldite 2014 adhesive, the cohesive failure (CF) and fiber tearing failures (LFT and TF) seen in macro images with the addition of HNT and boron nanoparticles support the improvement of the average shear strength and the adhesion performance between the adhesive and the substrates in SLJs.

3.2.2 | SEM Micrographs

The effects of varying amounts of doping particles on the material structure were evaluated by examining the fracture surfaces following the tensile test, as shown in Figure 7 (low-resolution SEM images) and Figure 8 (high-resolution images). SEM images provide crucial information on the textural and morphological properties of filled and pure samples, especially regarding interfacial bonds and overall adhesion. The fracture surface of the pure specimens (Figure 7a) was relatively smooth, typically indicating a more brittle failure. However, upon nanoparticle addition, the morphology of the damaged surfaces changed to a more irregular, rough, and complex texture, indicating a ductile fracture. This morphological evolution suggests that an enhanced interaction (interfacial bonding) between the adhesive matrix and the nanoparticles is crucial in improving the mechanical strength of the adhesive. The irregular fracture pattern, characterized by rough surfaces and more complex crack paths, indicates stronger interfacial bonding and increased resistance to crack propagation due to the fillers. The increase in roughness, evident in more crack formation on the fracture surface, increased mechanical resistance because it required more energy per unit area of crack.

Another difference in the fracture surfaces of pure and nanoparticle-doped samples lies in the size and number of pores (air bubbles). Importantly, air voids introduced during mixing were rigorously minimized using an effective additive incorporation technique followed by vacuum degassing at −0.75 bar and 22°C for approximately 10 min. The success of this process is reflected in the low standard deviation values in Table 5. As a result, the pores visible in SEM images mostly originate from interactions between the nanostructures and the adhesive during curing, rather than from preparation defects [57, 58]. These intrinsic defects include plastic voids caused by particle separation and, most significantly, matrix accumulation around particle clusters—a feature seen in specimens with excessive loading. Such localized microstructural defects significantly affect local stress distribution. Generally, the damaged surfaces exhibit a homogeneous structure, indicating that nanoparticles are well dispersed. SEM micrographs confirm that this uniformity is preserved across all compositions. Larger and more numerous pores in single HNT (2H) doped samples are believed to cause higher local stress (Figure 7b). In samples containing only nano-boron (4B), plastic voids from particle separation and many pores were observed (Figure 7c). Hybrid nanoparticle-added samples (Figure 7d–f) display irregular cracks, air gaps, and plastic voids on their damaged surfaces. Surface roughness increases with higher HNT ratios in hybrid-doped samples. The sample doped with 1.2% HNT and 0.3% BNP (12H3B) has a notably wrinkled surface with many irregular cracks. The additive matrix in this sample shows layered damage, including mud cracks. An image from the cohesive fracture region shows that the adhesive matrix fractured at significant elongation, consistent with the high elongation observed for the 12H3B sample in Figure 5. In the 15H3B sample, increasing the nanoparticle content leads to the adhesive matrix accumulating around particle clusters. This leads to reduced substrate wetting and the formation of pits on the damaged surface.

Figure 8 shows high-resolution SEM images of some samples reinforced with single-phase and hybrid nanoparticles. Since HNT particles are strong and more resistant to the adhesive matrix, they can prevent or guide the crack initiated in the matrix. When the applied shear load exceeds the adhesion strength between the HNTs and the polymer matrix, the HNTs embedded in the adhesive matrix are removed. The removed HNTs increase toughness by bridging crack surfaces and making crack propagation difficult [43]. The hollow, nanotube-like structure of the HNT particles, visible in Figure 8a, effectively bridges cracks due to their large aspect ratio, providing resistance to both crack opening and propagation. The formation of microcracks stabilized by HNT bridging helps prevent further crack propagation by dissipating fracture energy (Figure 8a). HNTs improve the fracture resistance of adhesive resin by stabilizing crack tips and inhibiting their easy propagation [59–61].

When the crack propagates through BNP particles, it deviates from its original path and bends; this mechanism, which increases toughness, is called the crack-deviation mechanism (Figure 8b). Another fracture mechanism is particle debonding followed by plastic void growth. The formation of many

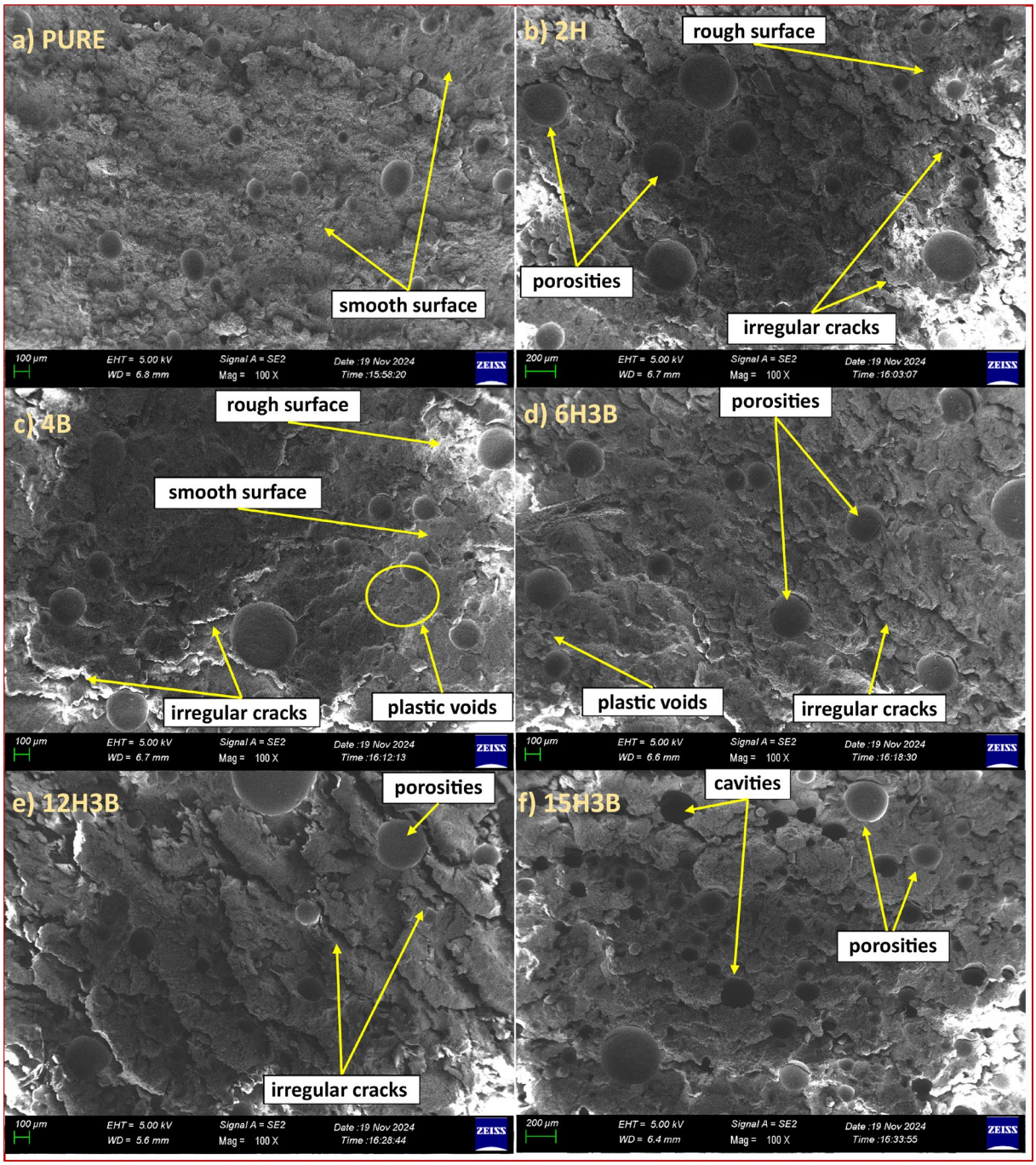

FIGURE 7 | Low-resolution SEM images of fracture surfaces: (a) Pure: Smooth brittle surface, (b) 2H: Rough surface; HNT-related crack-bridging, (c) 4B: Voids due to BNP debonding, (d) 6H3B: Irregular cracks and mixed voids, (e) 9H3B: Increased porosity and crack deviation, (f) 12H3B: Wrinkled, multilayered ductile fracture, (g) 15H3B: Agglomeration pits.

plastic voids throughout the matrix dissipates more energy and increases fracture resistance [39]. In general, particle additives are thought to improve adhesion strength by filling micro-voids on the substrate surface and creating new contact points [62] in the high-resolution SEM image of the sample doped with 1.2 wt.% HNT and 0.3 wt.% nano boron particles (12H3B); mechanisms such as crack-bridging, crack deflection, micro-crack formation, and particle separation increased the energy absorption by complicating fracture (Figure 8c). The synergistic effect of hybrid particles significantly increased the strength and toughness of the joints compared to single-phase specimens by deflecting cracks in three dimensions, thereby elongating the crack path and increasing energy consumption. The performance degradation observed in the 15H3B specimen is due to nanoparticle aggregation, as shown in Figure 8d.

3.3 | Fourier-Transform Infrared Spectroscopic Analysis

Fourier-transform infrared analysis helps explain how Araldite 2014 adhesives interact with BNPs and HNTs.

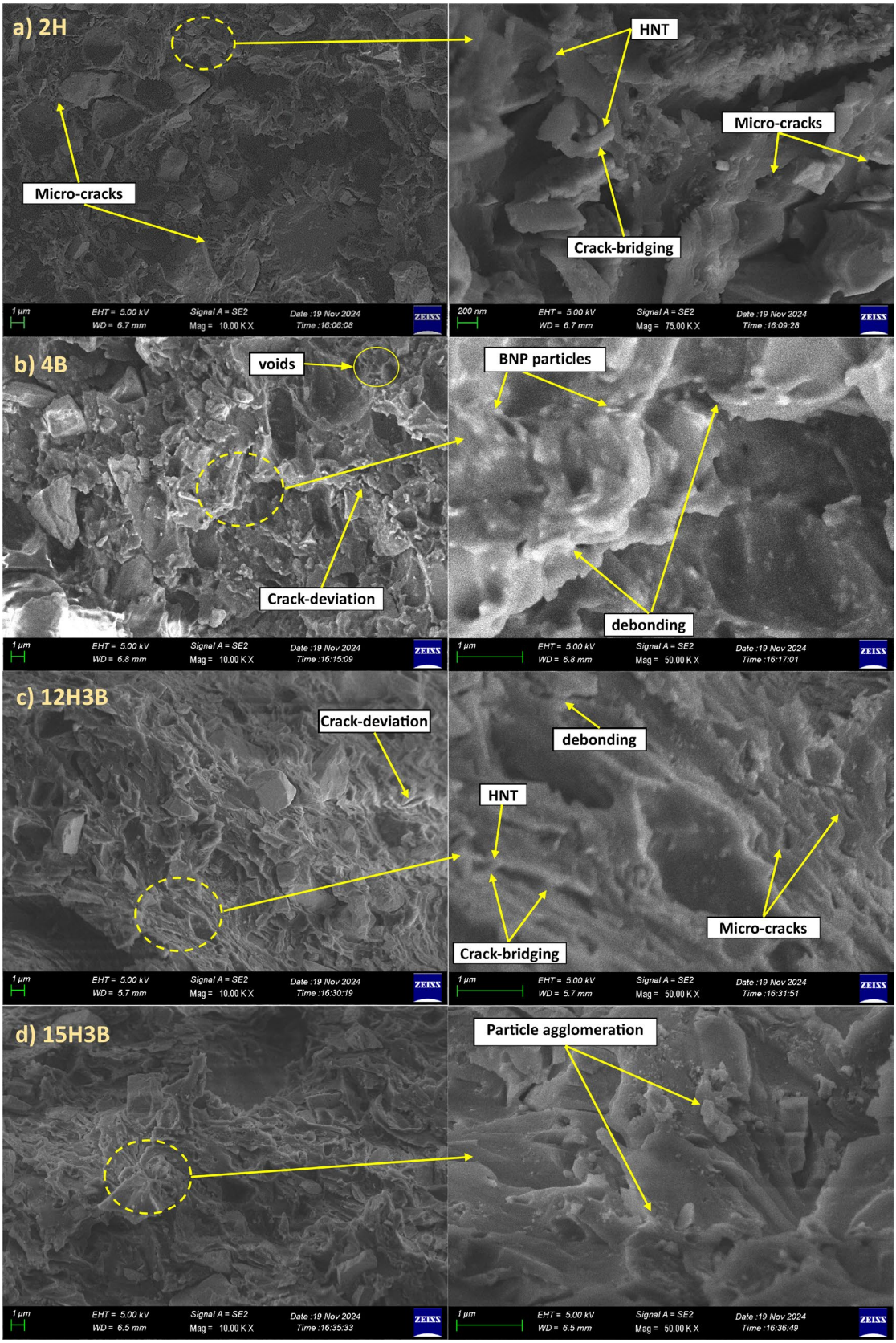

FIGURE 8 | High-resolution SEM images showing toughening mechanisms: (a) 2H: HNT crack-bridging, (b) 4B: Crack deviation and void growth, (c) 12H3B: Combined crack-bridging and deflection, (d) 15H3B: Agglomeration-induced brittle zones.

Figure 9 shows that the FTIR spectra exhibit clear shifts in peak positions and intensities, indicating that BNPs and HNTs are well distributed in the adhesive. Strong absorption bands between 1000 and 500 cm^{-1} match the Si—O and Al—O stretching vibrations typical of HNTs, as reported before [63, 64]. These bands persist after curing, indicating that

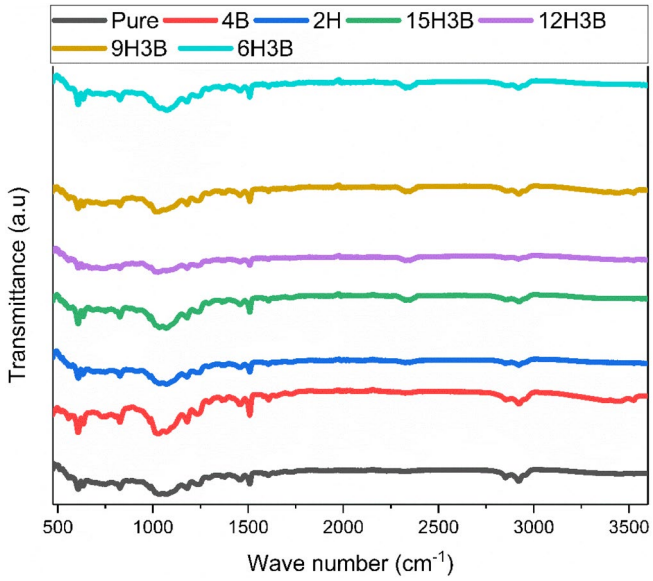

FIGURE 9 | FTIR spectra of adhesives.

HNTs remain chemically and physically part of the matrix and retain their structure. All modified samples also exhibit broader, stronger bands in the 1600–1700 cm^{-1} region, especially when more boron or HNT is present. These changes suggest increased chemical interactions and hydrogen bonding between the adhesive and the nanoparticles, which align with earlier studies on nanoparticle-reinforced polymers [65, 66]. Unique features in the 2300–2400 cm^{-1} region appear in all adhesives except the pure and 4B types. Recent studies link these to overtones or combination bands at reactive interfaces in epoxy/inorganic nanocomposites [67–69]. Their presence only in HNT-containing samples suggests more chemical activity at the HNT surfaces. This supports the idea that HNTs facilitate secondary crosslinking and the formation of oxygen-containing groups during curing [70], which aligns with the higher shear strength observed in the 2H-doped sample. Noticeable changes in the O—H and N—H stretching region (3600–3200 cm^{-1}), especially in the 12H3B and 15H3B samples, appear as broader, lower bands. These features are known signs of strong hydrogen bonding and polar interactions between the epoxy and the hydroxyl or amino groups on HNTs and boron particles [65–67]. These interactions improve nanoscale compatibility and increase crosslink density, thereby strengthening the composites. Overall, the changes in the 1600–1700, 2300–2400, and 3600–3200 cm^{-1} regions indicate that the additives are not only physically present but also participate in hydrogen bonding and chemical reactions at the interface. These molecular interactions help explain the better mechanical strength and adhesion seen in later tests, as shown by both FTIR and mechanical data [65, 70].

The spectral changes indicate that the additives are not only present in the adhesive but also participate in secondary interactions, hydrogen bonding, and reactions at the interface. These interactions explain the better mechanical properties and adhesion.

FTIR analysis was also used to detect any residual acetone, which served as a temporary solvent during sample preparation. The typical acetone peaks, like the strong C═O stretching band at 1700–1715 cm^{-1} and the CH_3 bending band near 1360 cm^{-1}, were not found in any cured samples. These bands are known markers for trace acetone in polymers [71–73], so their absence means all the acetone evaporated before curing. Gravimetric evaporation controls support this finding. Having no solvent left is important for accurate mechanical testing, as leftover solvents can soften the epoxy and reduce its strength. This means the FTIR data show that the improved mechanical properties in the composites come from the nanoparticle interactions, not from solvent effects.

4 | Conclusions

This study focused on creating single-lap joints using GFRP plates bonded with Araldite 2014-2 epoxy adhesive. Single-phase nanoparticles (HNT or BNP) and hybrid nanoparticles (a combination of both) were added at various ratios to enhance the adhesive's properties. The lap-shear tests were conducted on the prepared adhesive joints according to ASTM D5868-01, and the fracture surfaces were analyzed using macro- and SEM imaging. The key findings from the test results are summarized as follows:

- Both single-phase and hybrid additives were found to increase shear strength significantly. The average shear strength of the pure adhesive specimen was measured at 8.64 MPa. With the addition of 2% HNT (2H), shear strength improved by 31.3%, while the introduction of 0.4% BNP (referred to as 4B) resulted in a 28.76% increase.
- The highest strength increase was obtained in the 12H3B hybrid specimen containing 1.2% HNT and 0.3% BNP. This specimen achieved a remarkable 48.94% increase in shear strength compared to the pure specimen (12.86 MPa). This increase is 13.4% higher than the single-phase 2% HNT-doped specimen (2% H). The same specimen also increased the adhesive's ductility by 72.41%.
- The addition of nanoparticles also changed failure modes. Pure specimens primarily exhibited adhesion failure (AF), whereas specimens with added nanoparticles exhibited cohesive failure in the adhesive (CF) and fiber tearing in the GFRP (LFT/TF). This change indicates improved interfacial bonding between the adhesive and the substrates, particularly in the 12H3B specimen, which showed optimal healing properties.
- SEM analyses revealed that HNT particles increase toughness through mechanisms such as crack-bridging, and BNP particles increase toughness through crack-deviation and particle segregation. These mechanisms make fractures more difficult with a synergistic effect.
- FTIR analysis shows that between nanoparticles and araldite 2014 chemical reactions occur, and this improves the strength of the adhesive.

In conclusion, adding hybrid HNT and BNP particles to the adhesive at an appropriate rate exerted a crucial synergistic effect, improving mechanical performance—such as shear strength and toughness—more than adding a single phase of those

particles. The findings offer potential contributions to the development of high-performance adhesive formulations for structurally demanding applications.

Author Contributions

Gülağa Taş: conceptualization, investigation, writing – original draft, writing – review and editing, methodology, validation, visualization, software. **Mehmet Veysel Çakir:** conceptualization, investigation, writing – original draft, validation, methodology, visualization, writing – review and editing, software.

Conflicts of Interest

The authors declare no conflicts of interest.

Data Availability Statement

The data that supports the findings of this study are available in the supplementary material of this article.

References

1. A. J. Gunnion and I. Herszberg, "Parametric Study of Scarf Joints in Composite Structures," *Composite Structures* 75, no. 1–4 (2006): 364–376, https://doi.org/10.1016/j.compstruct.2006.04.053.

2. L. D. R. Grant, R. D. Adams, and L. F. M. da Silva, "Experimental and Numerical Analysis of Single-Lap Joints for the Automotive Industry," *International Journal of Adhesion and Adhesives* 29, no. 4 (2009): 405–413, https://doi.org/10.1016/j.ijadhadh.2008.09.001.

3. A. H. Makwana, A. A. Shaikh, A. K. Bakare, and S. Chitturi, "Investigation of Patch Hybridization Effect on the Composite Patch Repair of a Cracked Aluminum Plate: A Pragmatic Approach," *Mechanics of Advanced Materials and Structures* 26, no. 17 (2019): 1458–1468, https://doi.org/10.1080/15376494.2018.1432818.

4. A. R. Rasane, P. Kumar, and M. P. Khond, "Optimizing the Size of a CFRP Patch to Repair a Crack in a Thin Sheet," *Journal of Adhesion* 93, no. 13 (2017): 1064–1080, https://doi.org/10.1080/00218464.2016.1204236.

5. M. D. Banea and L. F. M. da Silva, "Adhesively Bonded Joints in Composite Materials: An Overview," *Proceedings of the Institution of Mechanical Engineers, Part L: Journal of Materials: Design and Applications* 223, no. 1 (2009): 1–18, https://doi.org/10.1243/14644207JMDA219.

6. J. Masson, M. Gigliotti, J.-C. Grandidier, J. Delozanne, W. Albouy, and N. Dagorn, "Numerical Method to Assess the Stress State and Gradients Induced by Thermo-Oxidation in Adhesively Bonded Joints for Aircraft Engine Applications," *International Journal of Adhesion and Adhesives* 113 (2022): 103063, https://doi.org/10.1016/j.ijadhadh.2021.103063.

7. G. Habenicht, *Applied Adhesive Bonding* (Wiley, 2008).

8. K. Turan and G. Örçen, "Failure Analysis of Adhesive-Patch-Repaired Edge-Notched Composite Plates," *Journal of Adhesion* 93, no. 4 (2017): 328–341, https://doi.org/10.1080/00218464.2015.1116984.

9. S. Akpinar, "Effects of Laminate Carbon/Epoxy Composite Patches on the Strength of Double-Strap Adhesive Joints: Experimental and Numerical Analysis," *Materials and Design* 51 (2013): 501–512, https://doi.org/10.1016/j.matdes.2013.04.037.

10. S. Akpinar, I. Hacısalihoglu, and A. Çalık, "The Effect of Geometry on Joint Strength in Adhesively Bonded Joints With the Same Adhesive Area," *Mechanics of Advanced Materials and Structures* 31, no. 12 (2024): 2635–2647, https://doi.org/10.1080/15376494.2022.2162641.

11. S. Akpinar, M. Kilbas, and M. Demiral, "Structural Tuning of Single-Lap Joints With Thin-Walled Inserts and Nanomodified Adhesives for Superior Flexural Performance," *Engineering Fracture Mechanics* 328 (2025): 111529, https://doi.org/10.1016/j.engfracmech.2025.111529.

12. F. Mottaghian and F. Taheri, "On the Flexural Response of Nanoparticle-Reinforced Adhesively Bonded Joints Mating 3D-Fiber Metal Laminates – A Coupled Numerical and Experimental Investigation," *International Journal of Adhesion and Adhesives* 120 (2023): 103278, https://doi.org/10.1016/j.ijadhadh.2022.103278.

13. M. V. Çakır, "The Synergistic Effect of Hybrid Nano-Silica and GNP Additives on the Flexural Strength and Toughening Mechanisms of Adhesively Bonded Joints," *International Journal of Adhesion and Adhesives* 122 (2023): 103333, https://doi.org/10.1016/j.ijadhadh.2023.103333.

14. F. C. Amorim, J. M. L. Reis, J. F. B. Souza, and H. S. da Costa Mattos, "Investigation of UV Exposure in Adhesively Bonded Single Lap Joints," *Applied Adhesion Science* 6, no. 1 (2018): 2, https://doi.org/10.1186/s40563-018-0103-6.

15. H. R. Gualberto, F. do Carmo Amorim, and H. R. M. Costa, "A Review of the Relationship Between Design Factors and Environmental Agents Regarding Adhesive Bonded Joints," *Journal of the Brazilian Society of Mechanical Sciences and Engineering* 43, no. 8 (2021): 389, https://doi.org/10.1007/s40430-021-03105-2.

16. M. A. Morgado, R. J. C. Carbas, E. A. S. Marques, and L. F. M. da Silva, "Reinforcement of CFRP Single Lap Joints Using Metal Laminates," *Composite Structures* 230 (2019): 111492, https://doi.org/10.1016/j.compstruct.2019.111492.

17. R. K. Behera, S. K. Parida, and R. R. Das, "Effect of Using Fibre Reinforced Epoxy Adhesive on the Strength of the Adhesively Bonded Single Lap Joints," *Composites. Part B, Engineering* 248 (2023): 110358, https://doi.org/10.1016/j.compositesb.2022.110358.

18. F. Delzendehrooy, M. R. Ayatollahi, A. Akhavan-Safar, and L. F. M. da Silva, "Strength Improvement of Adhesively Bonded Single Lap Joints With Date Palm Fibers: Effect of Type, Size, Treatment Method and Density of Fibers," *Composites. Part B, Engineering* 188 (2020): 107874, https://doi.org/10.1016/j.compositesb.2020.107874.

19. S. Akpinar, K. Demir, E. Gavgali, and A. F. Yetim, "A Study on the Effects of Nanostructure Reinforcement on the Failure Load in Adhesively Bonded Joints After the Subjected to Fully Reversed Fatigue Load," *Journal of Adhesion* 98, no. 13 (2022): 1972–1997, https://doi.org/10.1080/00218464.2021.1947811.

20. S. Akpinar, R. Sahin, A. Gürses, and I. A. Akpinar, "The Effect of Different Chemical Surface-Modified Carbon Fiber Structure and Ratio on Bond Strength in Adhesive Joints," *International Journal of Adhesion and Adhesives* 138 (2025): 103954, https://doi.org/10.1016/j.ijadhadh.2025.103954.

21. I. Avinc Akpinar, "A Study on the Effects of Electrochemical Oxidation and Silane Modification Applied to Fibers in Short Carbon Fiber-Reinforced Structural Adhesives and Adhesive Joints," *International Journal of Adhesion and Adhesives* 140 (2025): 104020, https://doi.org/10.1016/j.ijadhadh.2025.104020.

22. I. Avinc Akpinar, "The Effect of Chemical Etching and Nanostructure Additive Epoxy Coating Technique on Adhesion Strength in Aluminum Joints Bonded With Nanostructure Additive Adhesive," *International Journal of Adhesion and Adhesives* 129 (2024): 103584, https://doi.org/10.1016/j.ijadhadh.2023.103584.

23. D. De Cicco, Z. Asaee, and F. Taheri, "Use of Nanoparticles for Enhancing the Interlaminar Properties of Fiber-Reinforced Composites and Adhesively Bonded Joints—A Review," *Nanomaterials* 7, no. 11 (2017): 360, https://doi.org/10.3390/nano7110360.

24. P. Zamani, M. H. Alaei, L. F. M. da Silva, and D. Ghahremani-Moghadam, "On the Static and Fatigue Life of Nano-Reinforced Al-GFRP Bonded Joints Under Different Dispersion Treatments," *Fatigue and Fracture of Engineering Materials and Structures* 45, no. 4 (2022): 1088–1110, https://doi.org/10.1111/ffe.13652.

25. L. Zhai, G. Ling, J. Li, and Y. Wang, "The Effect of Nanoparticles on the Adhesion of Epoxy Adhesive," *Materials Letters* 60, no. 25–26 (2006): 3031–3033, https://doi.org/10.1016/j.matlet.2006.02.038.

26. H. Reza Borghei, B. Behjat, and M. Yazdani, "The Impact of Graphene Nanoparticle Additives on the Strength of Simple and Hybrid Adhesively Bonded Joints," *Journal of Composite Materials* 53, no. 23 (2019): 3335–3346, https://doi.org/10.1177/0021998318817588.

27. İ. Saraç, H. Adin, and Ş. Temiz, "Investigation of the Effect of Use of Nano-Al2O3, Nano-TiO2 and Nano-SiO2 Powders on Strength of Single Lap Joints Bonded With Epoxy Adhesive," *Composites. Part B, Engineering* 166 (2019): 472–482, https://doi.org/10.1016/j.compositesb.2019.02.007.

28. M. V. Cakir and D. Kinay, "MWCNT, Nano-Silica, and Nano-Clay Additives Effects on Adhesion Performance of Dissimilar Materials Bonded Joints," *Polymer Composites* 42, no. 11 (2021): 5880–5892, https://doi.org/10.1002/pc.26268.

29. I. A. Akpinar, K. Gültekin, S. Akpinar, H. Akbulut, and A. Ozel, "Experimental Analysis on the Single-Lap Joints Bonded by a Nanocomposite Adhesives Which Obtained by Adding Nanostructures," *Composites. Part B, Engineering* 110 (2017): 420–428, https://doi.org/10.1016/j.compositesb.2016.11.046.

30. G. Bali and T. Topkaya, "Effect of Graphene Nano-Particle Reinforcement on the Fatigue Behavior of Adhesively Bonded Single Lap Joints," *International Journal of Adhesion and Adhesives* 120 (2023): 103279, https://doi.org/10.1016/j.ijadhadh.2022.103279.

31. B. Soltannia and F. Taheri, "Influence of Nano-Reinforcement on the Mechanical Behavior of Adhesively Bonded Single-Lap Joints Subjected to Static, Quasi-Static, and Impact Loading," *Journal of Adhesion Science and Technology* 29, no. 5 (2015): 424–442, https://doi.org/10.1080/01694243.2014.991060.

32. S. Kemaloglu, G. Ozkoc, and A. Aytac, "Properties of Thermally Conductive Micro and Nano Size Boron Nitride Reinforced Silicon Rubber Composites," *Thermochimica Acta* 499, no. 1–2 (2010): 40–47, https://doi.org/10.1016/j.tca.2009.10.020.

33. M. Ghazizadeh, J. E. Estevez, E. T. Kimbro, and A. D. Kelkar, "Effect of Boron Nitride Nanoparticles on the Mechanaical Properties of Carbon Fiber Reinforced Polymeric Composites," *ASME International Mechanical Engineering Congress and Exposition* 46637 (2014): 38, https://doi.org/10.1115/IMECE2014-38342.

34. K. Gültekin and M. E. Yazici, "Mechanical Properties of Aluminum Bonded Joints Reinforced With Functionalized Boron Nitride and Boron Carbide Nanoparticles," *Proceedings of the Institution of Mechanical Engineers, Part L: Journal of Materials: Design and Applications* 236, no. 1 (2022): 37–49, https://doi.org/10.1177/14644207211056020.

35. S. S. Pasare and B. Suresha, "Mechanical and Tribological Properties of Carbon Fabric Reinforced Epoxy Composites With and Without Boron Nitride Filler," *AIP Conference Proceedings* 2236 (2020): 40005, https://doi.org/10.1063/5.0006937.

36. Ö. Özbek and M. V. Çakır, "MWCNT and Nano-Silica Hybrids Effect on Mechanical and Fracture Characterization of Single Lap Joints of GFRP Plates," *International Journal of Adhesion and Adhesives* 117 (2022): 103159, https://doi.org/10.1016/j.ijadhadh.2022.103159.

37. N. Razavi, M. R. Ayatollahi, A. Nemati Giv, and H. Khoramishad, "Single Lap Joints Bonded With Structural Adhesives Reinforced With a Mixture of Silica Nanoparticles and Multi Walled Carbon Nanotubes," *International Journal of Adhesion and Adhesives* 80 (2018): 76–86, https://doi.org/10.1016/j.ijadhadh.2017.10.007.

38. Q. Rao, H. Huang, Z. Ouyang, and X. Peng, "Synergy Effects of Multi-Walled Carbon Nanotube and Graphene Nanoplate Filled Epoxy Adhesive on the Shear Properties of Unidirectional Composite Bonded Joints," *Polymer Testing* 82 (2020): 106299, https://doi.org/10.1016/j.polymertesting.2019.106299.

39. P. Zamani, A. Jaamialahmadi, and L. F. M. da Silva, "The Influence of GNP and Nano-Silica Additives on Fatigue Life and Crack Initiation Phase of Al-GFRP Bonded Lap Joints Subjected to Four-Point Bending," *Composites. Part B, Engineering* 207 (2021): 108589, https://doi.org/10.1016/j.compositesb.2020.108589.

40. S. Tatiya, M. Pandey, and S. Bhattacharya, "Nanoparticles Containing Boron and Its Compounds—Synthesis and Applications: A Review," *Journal of Micromanufacturing* 3, no. 2 (2020): 159–173, https://doi.org/10.1177/2516598420965319.

41. M. V. Çakir, N. F. Doğan, and Ö. Özbek, "The Impact of Boron Nanoparticles on the Shear Performance and Damage Characteristics of Dissimilar Bonded Joints," *Physica Scripta* 100, no. 10 (2025): 105944, https://doi.org/10.1088/1402-4896/ae106a.

42. J.-H. Kim, H. J. Kim, D. Lee, et al., "Improvement Adhesion Durability of Epoxy Adhesive for Steel/Carbon Fiber-Reinforced Polymer Adhesive Joint Using Imidazole-Treated Halloysite Nanotube," *Advanced Composites and Hybrid Materials* 8, no. 1 (2025): 135, https://doi.org/10.1007/s42114-025-01224-1.

43. Ö. Özbek, M. V. Çakir, and N. F. Doğan, "Halloysit Nanotüp Katkısının Al-GFRP Tek Bindirmeli Yapıştırma Bağlantısında Kayma Dayanımına Etkisi," *Journal of Materials and Mechatronics: A* 3, no. 1 (2022): 117–128, https://doi.org/10.55546/jmm.1109990.

44. P. Yuan, D. Tan, and F. Annabi-Bergaya, "Properties and Applications of Halloysite Nanotubes: Recent Research Advances and Future Prospects," *Applied Clay Science* 112 (2015): 75–93, https://doi.org/10.1016/j.clay.2015.05.001.

45. N. A. Hanid, M. U. Wahit, Q. Guo, S. Mahmoodian, and M. Soheilmoghaddam, "Development of Regenerated Cellulose/Halloysites Nanocomposites via Ionic Liquids," *Carbohydrate Polymers* 99 (2014): 91–97, https://doi.org/10.1016/j.carbpol.2013.07.080.

46. S. Deng, J. Zhang, L. Ye, and J. Wu, "Toughening Epoxies With Halloysite Nanotubes," *Polymer* 49, no. 23 (2008): 5119–5127, https://doi.org/10.1016/j.polymer.2008.09.027.

47. K. Gültekin, S. Akpinar, A. Gürses, et al., "The Effects of Graphene Nanostructure Reinforcement on the Adhesive Method and the Graphene Reinforcement Ratio on the Failure Load in Adhesively Bonded Joints," *Composites. Part B, Engineering* 98 (2016): 362–369, https://doi.org/10.1016/j.compositesb.2016.05.039.

48. B. C. Smith, *Fundamentals of Fourier Transform Infrared Spectroscopy* (CRC Press, 2011).

49. Y. Li, C. Li, J. He, Y. Gao, and Z. Hu, "Effect of Functionalized Nano-SiO2 Addition on Bond Behavior of Adhesively Bonded CFRP-Steel Double-Lap Joint," *Construction and Building Materials* 244 (2020): 118400, https://doi.org/10.1016/j.conbuildmat.2020.118400.

50. B. Wetzel, F. Haupert, and M. Qiu Zhang, "Epoxy Nanocomposites With High Mechanical and Tribological Performance," *Composites Science and Technology* 63, no. 14 (2003): 2055–2067, https://doi.org/10.1016/S0266-3538(03)00115-5.

51. N. D. Alexopoulos, Z. Paragkamian, P. Poulin, and S. K. Kourkoulis, "Fracture Related Mechanical Properties of Low and High Graphene Reinforcement of Epoxy Nanocomposites," *Composites Science and Technology* 150 (2017): 194–204, https://doi.org/10.1016/j.compscitech.2017.07.030.

52. R. Bagheri, B. T. Marouf, and R. A. Pearson, "Rubber-Toughened Epoxies: A Critical Review," *Polymer Reviews* 49, no. 3 (2009): 201–225, https://doi.org/10.1080/15583720903048227.

53. ASTM, "D 5573–Standard Practice for Classifying Failure Modes in Fiber-Reinforced-Plastic (FRP)," (1999), ASTM Stand, 15, 3–5.

54. L. F. M. da Silva, A. S. O. Queirós Ferreira Barbosa, E. A. Sousa Marques, R. J. Camilo Carbas, and A. Ahkavan-Safar, *Adhesive Bonding Technology and Testing* (Wiley, 2023).

55. H. B. Kaybal and H. Ulus, "Comparative Analysis of Thermoplastic and Thermoset Adhesives Performance and the Influence on Failure Analysis in Jointed Elium –Based Composite Structures," *Polymer Composites* 45, no. 4 (2024): 3474–3492, https://doi.org/10.1002/pc.28003.

56. T. Wang, B. Gong, B. Wang, et al., "Relating the Failure Modes Transition to Plasma Treatment in Adhesively Bonded Carbon Fiber Composite Joints," *Composites Communications* 53 (2025): 102210, https://doi.org/10.1016/j.coco.2024.102210.

57. M. Al-Zu'bi, L. Anguilano, and M. Fan, "Effect of Incorporating Carbon- and Silicon-Based Nanomaterials on the Physico-Chemical Properties of a Structural Epoxy Adhesive," *Polymer Testing* 128 (2023): 108221, https://doi.org/10.1016/j.polymertesting.2023.108221.

58. S. Tamayo-Vegas, A. Muhsan, C. Liu, M. Tarfaoui, and K. Lafdi, "The Effect of Agglomeration on the Electrical and Mechanical Properties of Polymer Matrix Nanocomposites Reinforced With Carbon Nanotubes," *Polymers (Basel)* 14, no. 9 (2022): 1842, https://doi.org/10.3390/polym14091842.

59. Z. Murphy, M. Kent, C. Freeman, S. Landge, and E. Koricho, "Halloysite Nanotubes Functionalized With Epoxy and Thiol Organosilane Groups to Improve Fracture Toughness in Nanocomposites," *SN Applied Sciences* 2, no. 12 (2020): 2130, https://doi.org/10.1007/s42452-020-03909-2.

60. Y. Ye, H. Chen, J. Wu, and L. Ye, "High Impact Strength Epoxy Nanocomposites With Natural Nanotubes," *Polymer* 48, no. 21 (2007): 6426–6433, https://doi.org/10.1016/j.polymer.2007.08.035.

61. X. Mi, L. Zhong, F. Wei, et al., "Fabrication of Halloysite Nanotubes/Reduced Graphene Oxide Hybrids for Epoxy Composites With Improved Thermal and Mechanical Properties," *Polymer Testing* 76 (2019): 473–480, https://doi.org/10.1016/j.polymertesting.2019.04.007.

62. M. D. Banea, M. Rosioara, R. J. C. Carbas, and L. F. M. da Silva, "Multi-Material Adhesive Joints for Automotive Industry," *Composites. Part B, Engineering* 151 (2018): 71–77, https://doi.org/10.1016/j.compositesb.2018.06.009.

63. M. Tüfekci, T. Baytak, O. Bulut, et al., "Nonlinear Behaviour of Epoxy and Epoxy-Based Nanocomposites: An Integrated Experimental and Computational Analysis," *Mechanics Based Design of Structures and Machines* 52, no. 9 (2024): 6858–6888, https://doi.org/10.1080/15397734.2023.2293763.

64. H. Kang, X. Liu, S. Zhang, and J. Li, "Functionalization of Halloysite Nanotubes (HNTs) via Mussel-Inspired Surface Modification and Silane Grafting for HNTs/Soy Protein Isolate Nanocomposite Film Preparation," *RSC Advances* 7, no. 39 (2017): 24140–24148, https://doi.org/10.1039/C7RA02987J.

65. A. Boukaoud, Y. Chiba, and D. Sebbar, "A Periodic DFT Study of IR Spectra of Amino Acids: An Approach Toward a Better Understanding of the N-H and O-H Stretching Regions," *Vibrational Spectroscopy* 116 (2021): 103280, https://doi.org/10.1016/j.vibspec.2021.103280.

66. T. Bezrodna, G. Puchkovska, V. Shymanovska, J. Baran, and H. Ratajczak, "IR-Analysis of H-Bonded H2O on the Pure TiO2 Surface," *Journal of Molecular Structure* 700, no. 1–3 (2004): 175–181, https://doi.org/10.1016/j.molstruc.2003.12.057.

67. K.-Y. Hsiao, R.-J. Chung, P.-P. Chang, and T.-H. Tsai, "Identification of Hydroxyl and Polysiloxane Compounds via Infrared Absorption Spectroscopy With Targeted Noise Analysis," *Polymers* 17, no. 11 (2025): 1533, https://doi.org/10.3390/polym17111533.

68. D. S. Volkov, P. K. Krivoshein, and M. A. Proskurnin, "Detonation Nanodiamonds: A Comparison Study by Photoacoustic, Diffuse Reflectance, and Attenuated Total Reflection FTIR Spectroscopies," *Nanomaterials* 10, no. 12 (2020): 2501, https://doi.org/10.3390/nano10122501.

69. A. Nejad, X. Li, T. Zhu, Y. Liu, and C. Duan, "Mid-Infrared Laser Spectroscopy of Jet-Cooled Formic Acid Trimer: Mode-Dependent Line Broadening in the C–O Stretching Region," *Journal of Physical Chemistry Letters* 14, no. 35 (2023): 7795–7801, https://doi.org/10.1021/acs.jpclett.3c01860.

70. A. Buczek, K. Rzepiela, T. Kupka, and M. A. Broda, "Impact of O-H···π Hydrogen Bond on IR and NMR Parameters of Cannabidiol: Theoretical and Experimental Study," *Molecules* 30, no. 12 (2025): 2591, https://doi.org/10.3390/molecules30122591.

71. A. Almusa, A. H. S. Delgado, and A. M. Young, "Interpretation of ATR-FTIR Spectra of Dental Adhesives Throughout Simultaneous Polymerization and Solvent Loss," *PLoS One* 20, no. 6 (2025): e0325692, https://doi.org/10.1371/journal.pone.0325692.

72. A. Almusa, A. H. S. Delgado, P. Ashley, and A. M. Young, "Determination of Dental Adhesive Composition Throughout Solvent Drying and Polymerization Using ATR–FTIR Spectroscopy," *Polymers* 13, no. 22 (2021): 3886, https://doi.org/10.3390/polym13223886.

73. A. B. D. Nandiyanto, R. Ragadhita, and M. Fiandini, "Interpretation of Fourier Transform Infrared Spectra (FTIR): A Practical Approach in the Polymer/Plastic Thermal Decomposition," *Indonesian Journal of Science and Technology* 8, no. 1 (2022): 113–126, https://doi.org/10.17509/ijost.v8i1.53297.